Available online at www.sciencedirect.com
SCIENCE DIRECT®
ELSEVIER
Ultramicroscopy 98 (2004) 115–133
ultramicroscopy
www.elsevier.com/locate/ultramic

The contribution of phonon scattering to high-resolution images measured by off-axis electron holography

C.B. Boothroyd[a,*], R.E. Dunin-Borkowski[b]

[a] *IMRE, 3 Research Link, Singapore 117602, Singapore*
[b] *Department of Materials Science and Metallurgy, University of Cambridge, Pembroke Street, Cambridge CB2 3QZ, UK*

Received 6 June 2003; received in revised form 20 July 2003

Dedicated to Professor Fang-hua Li on the occasion of her 70th birthday

Abstract

The contribution of electrons that have been phonon scattered to the lattice fringe amplitude and the background intensity of a high-resolution electron microscope (HREM) image is addressed experimentally through the analysis of a defocus series of energy-filtered off-axis electron holograms. It is shown that at a typical specimen thickness used for HREM imaging approximately 15% of the electrons that contribute to an energy-filtered image have been phonon scattered. At this specimen thickness, the phonon-scattered electrons contribute a lattice image of opposite contrast to the elastic lattice image. The overall lattice fringe contrast is then reduced to 70% of the value that it would have in the absence of phonon scattering. At higher specimen thickness, the behaviour is defocus-dependent, with the phonon image having lattice fringe contrast of either the same or the opposite sense to the elastic image as the defocus is varied.

PACS: 61.14.Nm; 68.37.Lp

Keywords: Phonon scattering; Electron holography; High-resolution electron microscopy

1. Introduction

It is increasingly accepted that the lattice fringe contrast in experimental high-resolution electron microscope (HREM) images is lower than that in image simulations by a factor of between 2 and 6 [1,2]. For example, unfiltered HREM images of a thin crystal of WNbO were found to exhibit $\sim\frac{1}{4}$ of the contrast predicted by simulations, whereas similar energy-filtered images exhibited $\sim\frac{1}{2}$ of the predicted contrast [3]. The origin of this contrast discrepancy, which is commonly referred to as the "Stobbs factor", is still not understood [4,5]. Although electrons that have been scattered inelastically in the sample (with energy losses in excess of several eV) are known to add both lattice fringe contrast and a (relatively) uniform background to HREM images [6–9], neither of

*Corresponding author. Institute of Materials Research and Engineering, 3 Research Link, Singapore 117602. Tel.: +65-6874-4164; fax: +65-6872-0785.
E-mail address: chris-b@imre.a-star.edu.sg (C.B. Boothroyd).

0304-3991/$ - see front matter © 2003 Elsevier B.V. All rights reserved.
doi:10.1016/j.ultramic.2003.08.005

these effects is sufficient to account for the Stobbs factor, which is still present when zero-loss energy-filtered imaging (using an energy-selecting slit of several eV) is implemented [3]. A notable exception to these observations is the reported absence of a contrast discrepancy in energy-filtered HREM images of a 'clean' sample of sapphire [10].

It has been suggested that HREM image contrast may be affected significantly by phonon scattering, which is associated with the constant thermal motion of the specimen (even when it is cooled, due to zero-point energy) [11–13]. Phonon scattering results in the incident electron beam suffering energy losses of the order of kT ($\sim$0.025 eV at room temperature). Traditionally, its effect on images and diffraction patterns has been included in simulations by using a Debye–Waller factor, which attenuates high-angle scattering and models the blurring of atoms due to their thermal motion. However, this approach does not take into account the contribution of the phonon-scattered electrons to the image or the diffraction pattern. A better approximation is provided by frozen phonon calculations, which involve displacing atoms from the perfect lattice for the purpose of the simulation. These displacements can be either uncorrelated (the "Einstein model") [14] or correlated (the "Debye model") [15,16].

A lower limit to the contribution of phonon-scattered electrons to an HREM image has been provided by measuring the intensity of the diffuse scattering between the Bragg spots in a convergent beam electron diffraction pattern of a 25-nm thick Si sample [5]. On the assumption that the phonon-scattered electrons were uniformly distributed in the diffraction pattern, and that phonon scattering adds only a constant background intensity to the lattice image, the results suggested that $\sim$5% of the electrons in the image had been phonon scattered, which would not account for a contrast reduction by a factor of 2 or 3. However, phonon scattering is in practice expected to be concentrated at diffraction spots [12], suggesting firstly that this measurement is an underestimate and secondly that phonon-scattered electrons may in fact provide lattice fringe contrast that can either add to or subtract from the elastic lattice fringe image.

In this paper, we use off-axis electron holography as an alternative experimental approach to measure the contribution of phonon scattering to an HREM image. In electron holography, an electron biprism is used to interfere an electron wave that has passed through the specimen with a different part of the same electron wave (the "reference" wave) that has passed only through vacuum [17]. Analysis of the resulting holographic interference fringe pattern is used to recover both the amplitude and the phase shift of the electron wave that has passed through the specimen (and through the objective lens of the microscope). Interference can only occur between parts of the electron wave that have the same energy to within $\sim 10^{-15}$ eV [18,19] (although see Ref. [20] for an alternative argument). Therefore, electrons that have lost energy due to phonon scattering in the specimen cannot interfere with the vacuum reference wave, and cannot contribute to the wave function reconstructed from the "sideband" of the electron hologram [21]. However, they do contribute to the intensity of a normal HREM image, which can be recovered from the "centreband" of the same hologram (see below). As a result, it is possible to obtain, from a single electron hologram, both a normal lattice image and a lattice image from which all inelastic scattering (including phonon scattering) has been removed. In order to ensure that the normal lattice image contains only phonon scattering and not contributions to the contrast from electrons that have suffered higher energy losses, the hologram must be recorded using an energy filter. Additional information about the behaviour of phonon scattering with objective lens defocus can then be obtained by acquiring a defocus series of energy-filtered high-resolution electron holograms. This has been our approach in this paper.

2. Experimental details

Energy-filtered defocus series of high-resolution electron holograms were acquired at an accelerating voltage of 297 kV from a sample of ZrB_{12} using a Philips CM300 field emission gun (FEG) transmission electron microscope equipped with

a SuperTwin objective lens ($C_s = 1.2$ mm), a Gatan imaging filter and a 2048 pixel charge-coupled device (CCD) camera. ZrB_{12}, whose crystal structure is described elsewhere [22,23], was chosen for analysis primarily because this material has a large lattice parameter of 0.74 nm. As a result, the lattice fringes are well within the resolution limit of the electron microscope, their visibility is unlikely to be affected by slight instabilities of the imaging system, and the biprism voltage required to sample each lattice fringe with several holographic fringes is not excessive. A further advantage is that the specimen could be prepared simply by crushing it onto a holey carbon film, which allowed sample preparation artefacts associated with ion-beam milling to be eliminated. Defocus series of electron holograms, of which a representative example is shown in Fig. 1a, were acquired from a small crystal of ZrB_{12} that had been tilted to the [0 0 1] orientation of the cubic F structure (space group Fm3m). An objective aperture of semi-angle 26 mrad (13 nm^{-1}) was used to limit stray scattering. A Digital Micrograph script allowed the automated acquisition of an unfiltered electron hologram close to Gaussian focus (with the energy-selecting slit of the imaging filter removed), followed by a defocus series of ten energy-filtered electron holograms (using a 10 eV energy-selecting slit) from near Gaussian defocus towards underfocus in steps of $\sim$10 nm, and finally an energy-filtered hologram at the starting defocus. The absolute defocus value of each image was determined by using the phase correlation and focal series reconstruction method of Meyer et al. [24]. The interference fringe spacing in each hologram was 0.089 nm. Additional holograms that had been acquired from vacuum alone were always used to remove distortions associated with the imaging and recording system.

In the present study, no attempt was made to compare the experimental results with image simulations. In order to perform reliable simulations, all of the parameters that describe the specimen and the electron optics, including the specimen thickness, the crystal tilt and the beam tilt, must be known independently. Of these parameters, the beam tilt can be determined from a tilt series of images, while the local crystal tilt

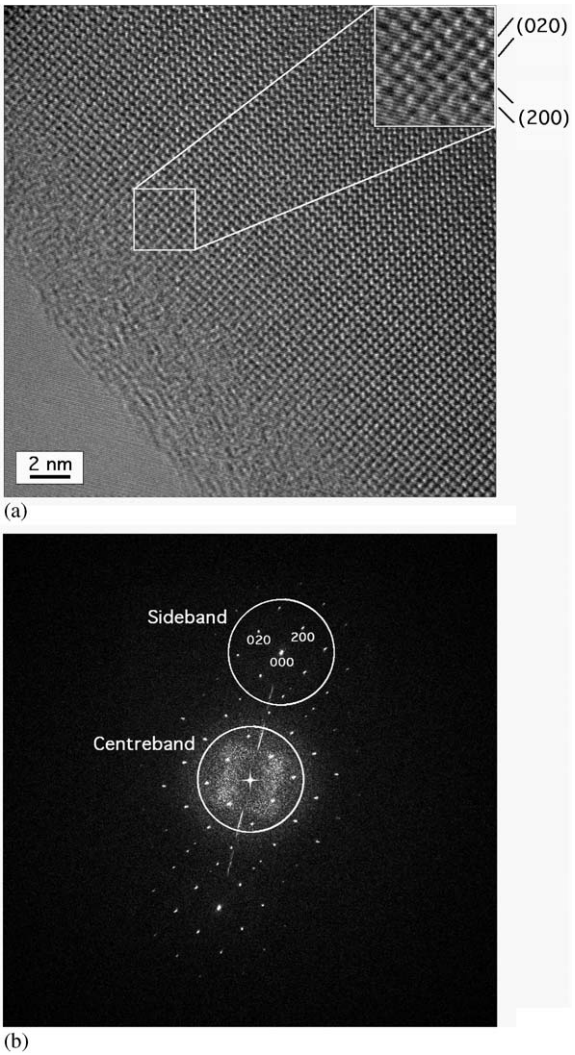

Fig. 1. (a) One member of a defocus series of energy-filtered electron holograms of a ZrB_{12} crystal oriented close to a [0 0 1] zone axis. The inset enlargement shows the holographic interference fringes and the (2 0 0) and (0 2 0) lattice fringes of ZrB_{12}. (b) Fourier transform of the hologram in (a), with the "centreband" and "sideband" marked. The two circles show the sizes of the apertures used when reconstructing the lattice images shown in Figs. 2e and f.

may be estimated from the relative intensities of the diffraction maxima in the sideband. However, because of the nature of the present specimen, it was not possible to determine the specimen thickness independently. Although the specimen thickness could be estimated by matching the

experimental images to simulations, this approach was not used because there is an inherent danger in allowing the specimen thickness to become a "free parameter" in such a match.

3. Analysis

The electron wave function that has passed through the specimen and the microscope objective lens can be written in the form

$$\psi(\boldsymbol{r}) = A(\boldsymbol{r})\exp[\mathrm{i}\phi(\boldsymbol{r})], \quad (1)$$

where $\boldsymbol{r}$ is a vector perpendicular to the incident electron beam and $A(\boldsymbol{r})$ and $\phi(\boldsymbol{r})$ represent the amplitude and the phase shift of the wave function, respectively. If an off-axis electron hologram is formed by superimposing a reference wave (that has passed only through vacuum) onto the specimen wave specified by Eq. (1), then the intensity of this hologram is given by the expression

$$I_{\mathrm{hol}}(\boldsymbol{r}) = |\psi(\boldsymbol{r}) + \exp[2\pi\mathrm{i}\boldsymbol{q}_{\mathrm{c}}\cdot\boldsymbol{r}]|^2, \quad (2)$$

$$I_{\mathrm{hol}}(\boldsymbol{r}) = 1 + A^2(\boldsymbol{r}) + 2A(\boldsymbol{r})\cos[2\pi\mathrm{i}\boldsymbol{q}_{\mathrm{c}}\cdot\boldsymbol{r} + \phi(\boldsymbol{r})], \quad (3)$$

where the wave vector $\boldsymbol{q}_{\mathrm{c}}$ describes the tilt of the reference wave with respect to the specimen wave, The Fourier transform of the resulting electron hologram is simply

$$\begin{aligned}\mathrm{FT}[I_{\mathrm{hol}}(\boldsymbol{r})] = {} & \delta(\boldsymbol{q}) + \mathrm{FT}[A^2(\boldsymbol{r})] \\ & + \delta(\boldsymbol{q}+\boldsymbol{q}_{\mathrm{c}})\otimes\mathrm{FT}[A(\boldsymbol{r})\exp[\mathrm{i}\phi(\boldsymbol{r})]] \\ & + \delta(\boldsymbol{q}-\boldsymbol{q}_{\mathrm{c}})\otimes\mathrm{FT}[A(\boldsymbol{r})\exp[-\mathrm{i}\phi(\boldsymbol{r})]]. \quad (4)\end{aligned}$$

The first two terms in Eq. (4), which are centred on the origin in Fourier space and represent the "centreband", describe the Fourier transforms of the reference and specimen images, respectively. The last two terms describe the Fourier transforms of the specimen image wave and its complex conjugate (the "sidebands"), which are centred at positions $\boldsymbol{q}=-\boldsymbol{q}_{\mathrm{c}}$ and $\boldsymbol{q}=+\boldsymbol{q}_{\mathrm{c}}$ in Fourier space, respectively.

Electron holograms were analysed with reference to Eqs. (1)–(4) using the procedure outlined in Figs. 1 and 2. The "centreband" in the Fourier transform of each hologram (Fig. 1b), which is represented by the first two terms in Eq. (4), was used to generate a normal lattice image by using a Fourier filter of radius 4.8 nm^{-1} (containing only the 000, 200 and 220 reflections) to exclude the information in the sidebands (i.e., to exclude the holographic interference fringes). The streak associated with Fresnel fringes from the biprism wire, which is visible in Fig. 1b, was also removed by Fourier filtering at this stage. The additional contribution to the intensity of the lattice image from the reference wave, which is equal to half of the total intensity in the vacuum region outside the edge of the sample, was removed by subtracting half of the mean intensity in the vacuum region from the entire lattice image, and then rescaling the result to a vacuum intensity of unity. This procedure is summarised in Figs. 2a and e. One of the sidebands in the hologram was analysed in a similar way to form a "sideband" lattice image, in this case from the square of the reconstructed amplitude (Figs. 2b-d and f). The sideband lattice image was also scaled so that the vacuum region had an intensity of unity.

Because the centreband and sideband images (Figs. 2e and f) are obtained from the same area of the same hologram, they are always in perfect registry. Assuming perfect coherence of the incident electron beam and negligible specimen vibration (see below), the difference between these

Fig. 2. Stages involved in the determination of mean intensity and lattice fringe amplitude profiles from holograms such as that shown in Fig. 1a. (a) and (b) show the centreband and sideband of the Fourier transform in Fig. 1b. (c) and (d) show the amplitude and phase of the hologram reconstructed from the sideband. (e) is a lattice image reconstructed from the centreband, after the intensity of the hologram reference wave has been subtracted. (f) is a lattice image calculated from the square of the amplitude image reconstructed from the sideband. (g) shows the Fourier transform of either the centreband or the sideband lattice image, and the masks applied to the Fourier transform for the subsequent steps in the procedure. (j) shows the mean intensity of the lattice image, calculated by applying a mask to the 000 beam in (g). A similar mask applied to the 200 beam in (g) provides the amplitude (h) and phase (i) of the 200 lattice fringes. After high-pass filtering the phase, the resulting amplitude and phase are shown in (k) and (l). The mean intensities and amplitudes of the lattice images in (e) and (f), which are projected parallel to the edge of the sample in (j) and (k), are shown in the form of line profiles in (m) and (n).

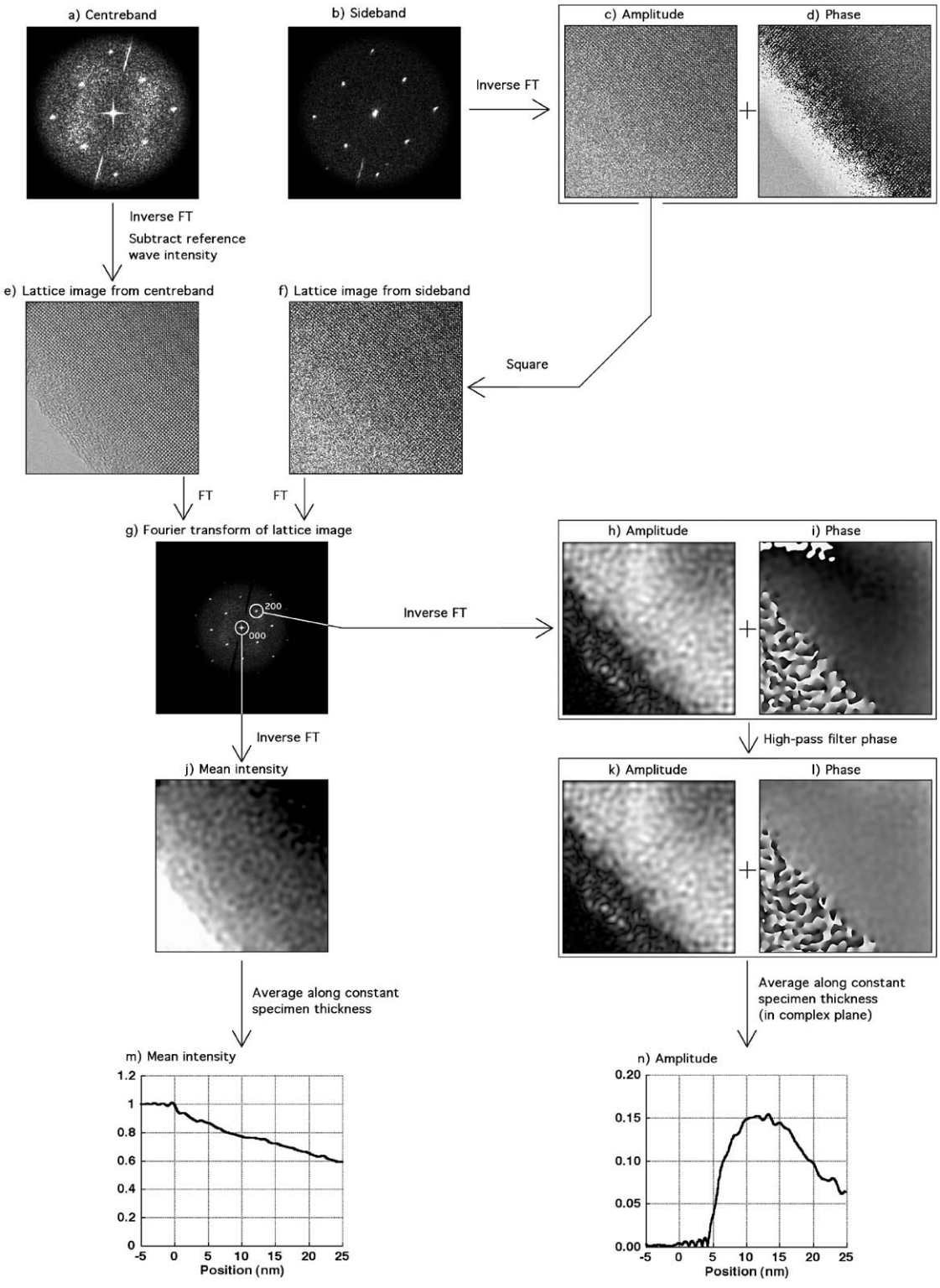
a) Centreband
b) Sideband
Inverse FT
c) Amplitude
d) Phase
Inverse FT
Subtract reference wave intensity
e) Lattice image from centreband
f) Lattice image from sideband
Square
FT
FT
g) Fourier transform of lattice image
200
000
Inverse FT
h) Amplitude
i) Phase
High-pass filter phase
Inverse FT
j) Mean intensity
k) Amplitude
l) Phase
Average along constant specimen thickness
Average along constant specimen thickness (in complex plane)
m) Mean intensity
1.2
1
0.8
0.6
0.4
0.2
0
-5 0 5 10 15 20 25
Position (nm)
n) Amplitude
0.20
0.15
0.10
0.05
0.00
-5 0 5 10 15 20 25
Position (nm)

two images is in principle a direct measure of the phonon scattering contribution to an HREM image. However, this difference image cannot be evaluated directly because the sideband image recovered from an electron hologram is always very noisy [25]. As a result, averaging methods, which are described below, must be used to reduce the noise before the centreband and sideband images can be compared. Although it would be possible to make use of the phase information in the reconstructed image waves, which is less noisy, by determining the exit surface wave function from the entire defocus series of electron holograms and then recalculating the amplitude at each defocus, we have chosen to use the amplitude images alone because they can be compared directly with the corresponding centreband images. This procedure removes the possibility of additional errors being introduced during the wave function reconstruction process.

In order to compare the centreband and sideband lattice images (Figs. 2e and f), both the mean intensity of each image and the lattice fringe amplitude were plotted as a function of specimen thickness. The mean intensity (Fig. 2j) was calculated by using a mask of radius $0.87\,\mathrm{nm}^{-1}$ to exclude all but the 000 beam from the Fourier transform of the image (Fig. 2g). Because the edge of the specimen was straight in the region of interest, the resulting image could be averaged parallel to this direction in order to obtain a line profile of mean intensity as a function of specimen thickness (Fig. 2m). In order to evaluate the amplitudes of the 200 and 020 lattice fringes, the same circular mask was applied to the peak corresponding to the lattice fringe of interest, this peak was shifted to the origin and then inverse Fourier transformed. The amplitude of the resulting complex image provided a measure of the amplitude of the corresponding lattice fringes, while the phase provided a measure of the variation in their position across the image.

The effect of the modulation transfer function (MTF) of the CCD camera on the lattice fringe amplitudes was also considered carefully. Based on an MTF curve that had been measured previously for an identical camera [26], the amplitudes of the 200 and 020 lattice fringes in the centreband lattice images are reduced by a factor of 0.85 from their true values. A correction for this factor was made after the amplitudes had been calculated. The holographic interference fringes are reduced in amplitude much more strongly (in this case by a factor of 0.41). This factor (and any other reduction in fringe contrast) was taken into account by using an additional hologram acquired from vacuum alone during the reconstruction process, as well as by scaling the vacuum part of the resulting sideband amplitude to unity. The effect of the asymmetry (the slope) of the MTF across the position of the sideband is small because, for example, the 200 lattice fringe amplitude depends on both the 200 and the $\bar{2}00$ peaks, which are on either side of the centre of the sideband. To first order, the effect of the higher value of the MTF on one side of the sideband cancels out the lower value on the other side.

A further complication arises from the fact that the amplitude images derived from the sidebands are very noisy. As a result, they cannot be projected parallel to the specimen edge directly to provide line profiles of the amplitude as a function of specimen thickness (line A in Fig. 3), as this procedure only works reliably when the lattice fringe amplitude is significant when compared to the noise in the image. Unfortunately, both close to the sample edge and outside the sample, the noise in the amplitude image is always positive. No matter how large an area is averaged, the result is therefore positive even if no lattice fringes are present. This problem can be overcome by performing the average in the complex plane before calculating the amplitude. The phase of the reconstructed wave function is random in these regions, and approximately constant in the crystalline parts of the specimen. When the averaging is carried out in the complex plane, the noise in the vacuum is now closer to zero, as shown in line B in Fig. 3. A disadvantage of this approach is that, as well as reducing the noise in the vacuum, the amplitude is also reduced at a distance of between 8 and 18 nm from the sample edge because the lattice fringes are not quite straight in this region, perhaps because of small variations in crystal tilt. This slight bending of the lattice fringes corresponds to a slow variation in phase, which can be

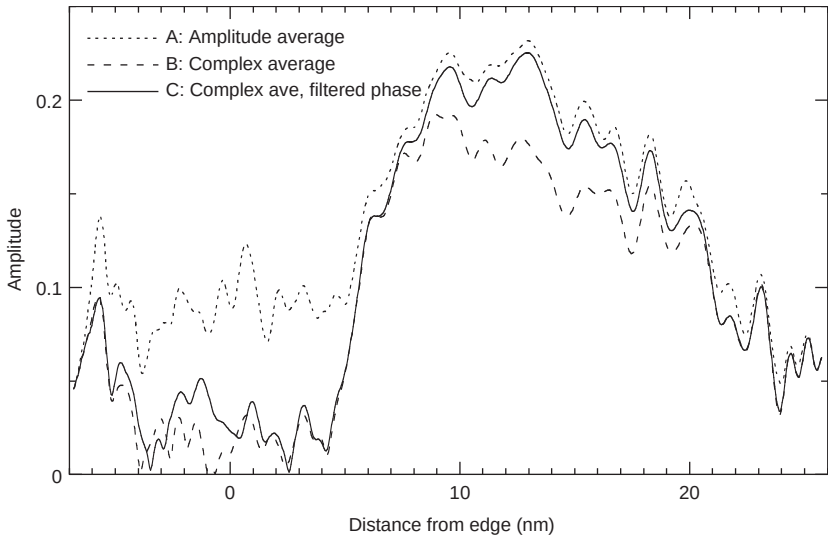

Fig. 3. Illustration of different methods of averaging lattice fringe amplitudes. Line A is a simple average of the lattice fringe amplitude, such as that shown in Fig. 2h, parallel to the specimen edge. In the amorphous layer and outside the sample, the noise always averages to a positive value. Line B is an average evaluated in the complex plane, taking into account both the amplitude (Fig. 2h) and the phase (Fig. 2i) of the lattice fringes. Line C is also an average in the complex plane, evaluated after the phase has been high-pass filtered (Fig. 2l) to compensate for the lattice fringes not being exactly straight.

removed by high-pass filtering the phase image before performing the average in the complex plane, as shown in line C in Fig. 3. The average amplitude is now similar to line A in the crystalline regions and almost as low as line B in the vacuum region. This method, which is summarised in Figs. 2g-i, k, l and n, was used to calculate the plots of average lattice fringe amplitude that are described below.

A final issue, which was pointed out to the authors by Dr R. R. Meyer but whose assessment is beyond the scope of this paper, is associated with the different ways in which the effects of spatial and temporal coherence affect the recovery of amplitude information from the centreband and the sideband of an electron hologram. A significant problem arises here because analysis of the centreband provides a sum of image *intensities* for different beam tilts and defocus values (describing the effects of spatial and temporal coherence), as for a conventional high-resolution image, whereas the sideband is formed from a sum of holographic fringes whose position and amplitude depend on the beam tilt and defocus. The effect of this difference on the recovered amplitude (and in particular on its mean value) is both difficult to establish and unknown at present, and will be discussed in detail in a separate study. A preliminary study by Dr. R.R. Meyer suggests that our measurements of the mean intensity from the sideband images are slightly low, while our measurements of lattice fringe amplitude are affected very little by spatial and temporal coherence.

4. Definitions and predictions

The mean intensities and the amplitudes calculated from the sideband images contain only elastic scattering, while those from the centreband images also contain contributions from phonon-scattered electrons. Before examining the experimental results, it is worth considering the different ways in which phonon scattering may be expected to affect the experimental plots of mean intensity, lattice fringe amplitude and lattice fringe contrast, as well as to provide a strict definition of the

term "contrast", which is used in many different contexts in electron microscopy.

Although lattice fringe contrast can be defined as the standard deviation of an image divided by its mean value, it is then influenced by noise in the image. Here, we measure the *amplitudes* of specific lattice fringes using the Fourier filtering approach described above, which are affected less by noise. We also use a similar Fourier filtering approach to measure the mean intensity of the image. We then define the *contrast* of the lattice fringes as the lattice fringe amplitude divided by the mean intensity. Fig. 4 shows schematically how plots of mean intensity, lattice fringe amplitude and lattice fringe contrast may be expected to vary on the basis of four different assumptions of the effect of phonon scattering on the image. Fig. 4a illustrates the fact that the addition of a uniform background intensity to the entire centreband image, for example from stray scattering in the electron microscope column, would add a constant level, b, to the mean intensity, but would not affect the lattice fringe amplitude (middle column). After scaling the vacuum regions in both images to unity (bottom row, Fig. 4a), the sideband amplitude would be higher than that of the centreband by a factor of $1/(1+b)$ (middle column). The lattice fringe contrast would also increase correspondingly. A more likely scenario is that the amount of phonon scattering increases with specimen thickness and adds a background to the elastic image. In this case, which is shown in Fig. 4b, the sideband and centreband amplitudes are identical, and the lattice fringe contrast (right column) is higher in the sideband image. Two other possible effects of phonon scattering are shown in Figs. 4c and d. In Fig. 4c, it is assumed that the phonon-scattered electrons contribute lattice fringes that are identical to those in the elastic image. The lattice fringe *contrast* is then the same for the sideband and centreband images, while the lattice fringe *amplitude* is higher for the centreband image. Conversely, if the phonon-scattered electrons produce a lattice image that is of opposite sense to the elastic image (Fig. 4d), then the lattice fringe amplitude and contrast are both lower for the centreband image than for the sideband image.

5. Experimental results

5.1. Mean intensity

The mean intensities of the centreband images were found to be similar to each other when calculated from different members of the defocus series of electron holograms, and likewise for the mean intensities of the sideband images. As a result, the centreband and sideband mean intensities were averaged over each defocus series, and are plotted in Fig. 5 alongside a similar line profile obtained from the unfiltered image. Differences between these three profiles were used to infer the inelastic (excluding phonon) contribution to the images (from the difference between the unfiltered and elastic mean intensities), and the phonon contribution alone (from the difference between the energy-filtered centreband and sideband mean intensities). From these profiles, which are also shown in Fig. 5, it can be seen that inelastic scattering makes a significant contribution to the mean intensity of an unfiltered HREM image, even in the thinnest regions of the sample. However, much of this inelastic scattering originates in the amorphous layer on the sample surface, within which $\sim 7\%$ of the scattering is inelastic. It is particularly interesting to notice that very little phonon scattering contributes to the image intensity in the amorphous region at the edge of the sample. Instead, the proportion of phonon scattering that contributes to the image increases steadily from the edge of the crystalline region, up to a value of 11% (which is an upper limit due to the effects of spatial and temporal coherence discussed above) at a distance of 15 nm from the specimen edge. At this thickness, which is typical of that used in HREM imaging, 11% of the electrons have been lost outside the objective aperture, 17% have been scattered inelastically, and up to 11% have been scattered by phonons, leaving only 61% purely elastically scattered and retained within the chosen objective aperture. Although it has not been possible to determine the thickness of the specimen absolutely, at this stage the results suggest that the proportion of phonon-scattered electrons is not on its own sufficient to explain a reduction in lattice fringe

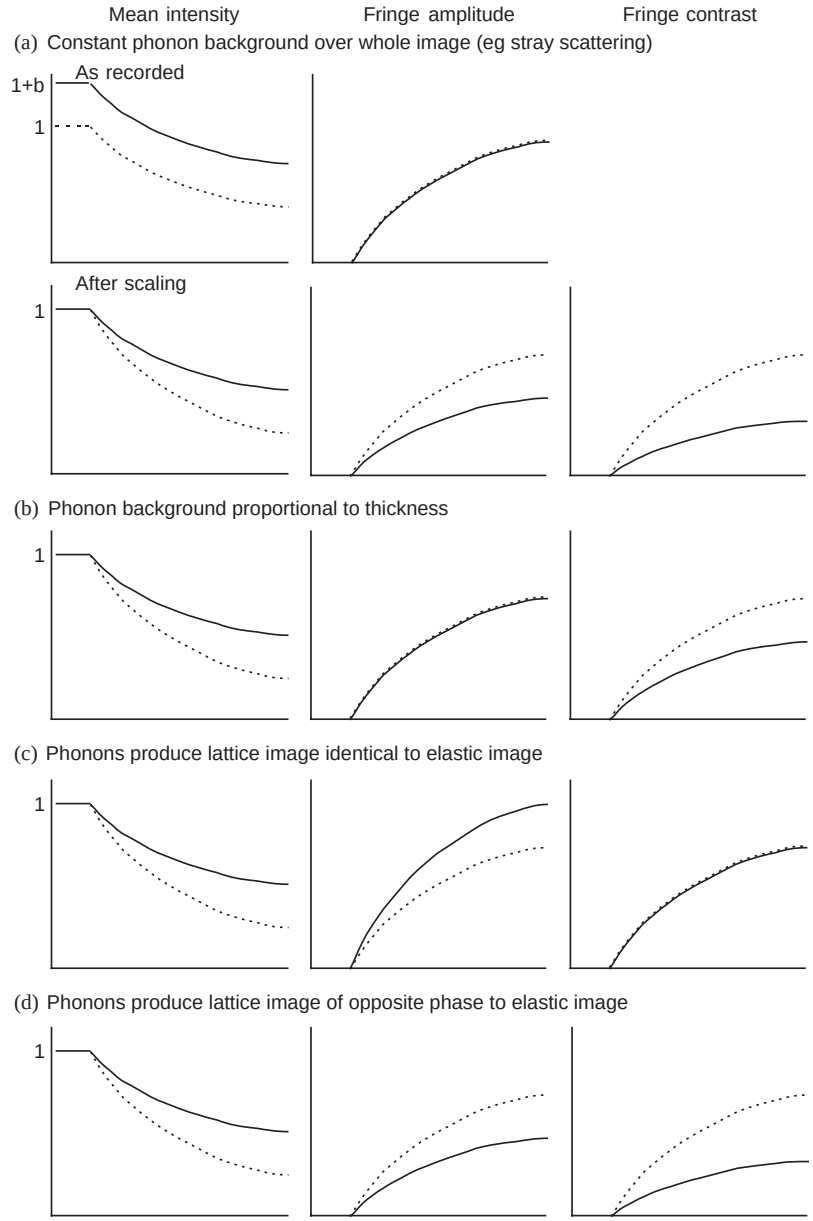

Fig. 4. Schematic diagrams showing the possible effect of phonon scattering on plots of mean intensity (left column), lattice fringe amplitude (middle column) and lattice fringe contrast (right column). The solid lines are plotted for the centreband images and thus contain both elastic and phonon scattering, while the dotted lines are for the sideband images and so contain only elastic scattering. (a) shows the effect of the addition of a uniform background, b, to the entire image. The top row of (a) shows the recorded mean intensity and lattice fringe amplitude, while the bottom row shows the result after the vacuum region has been scaled to unity. (b) illustrates the addition of a phonon background (i.e., containing no lattice fringes) that is proportional to specimen thickness. The phonon background does not affect the lattice fringe amplitude, but the lattice fringe contrast in the sideband images is higher as a result of the decrease in mean intensity. (c) shows the addition of a phonon lattice image that is identical to the elastic lattice image. The measured lattice fringe amplitude is now higher in the centreband image, but the lattice fringe contrast is the same in the centreband and sideband images. (d) shows the addition of a phonon lattice image of opposite sense to the elastic lattice image. The lattice fringe amplitude in the centreband image is now lower than that in the sideband image.

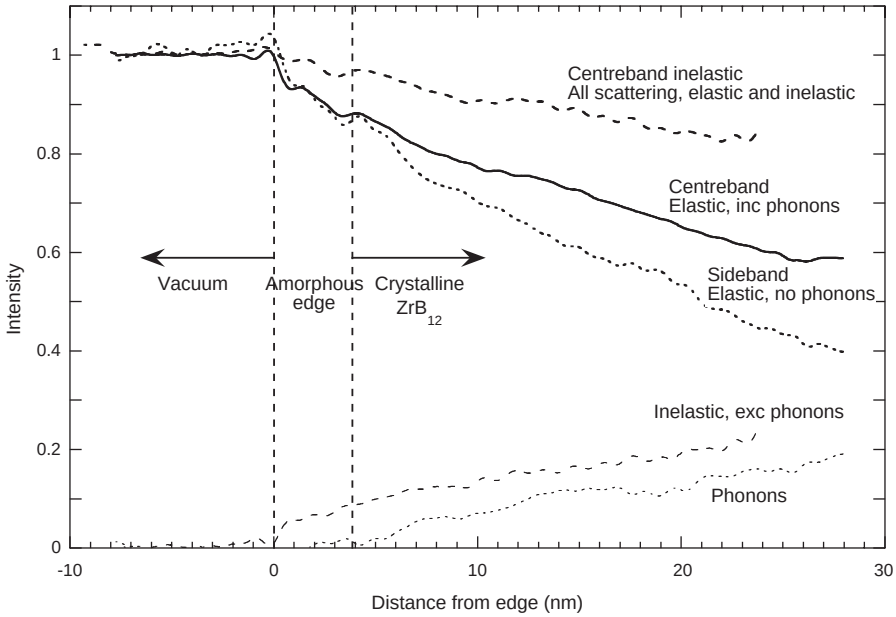

Fig. 5. Mean intensities of the centreband images, sideband images and an unfiltered image plotted as a function of the distance from the specimen edge. Also plotted are the inelastic contribution to the unfiltered image, evaluated from the difference between the unfiltered and centreband profiles, and the phonon contribution to an energy-filtered (centreband) image, evaluated from the difference between the centreband and sideband profiles. Differences between the effects of spatial and temporal coherence on the mean intensities recovered from the centreband and the sideband have not been considered when generating these plots.

contrast by a factor of two or three from that in image simulations.

5.2. *Lattice fringe amplitude and contrast*

Calculations in the literature suggest that phonon-scattered electrons may retain lattice fringe contrast [11–13]. This is indeed the case for high-angle dark-field imaging, which is dominated by phonon scattering [14, 27]. Figs. 6a and b show the amplitudes of the 200 and 020 lattice fringes, respectively, in the centreband (solid line) and sideband (dotted line) images for all ten defocus values. There are significant differences between the centreband and sideband amplitudes, in addition to the expected rapid variation in lattice fringe amplitude with both specimen thickness and defocus. The averages of the profiles in each of Figs. 6a and b, which were evaluated over all defocus values and are shown in Fig. 7, provide a better idea of the overall specimen thickness-dependence of the amplitude. At low specimen thickness, the sideband amplitude is on average higher than the centreband amplitude. However, in thicker regions of the specimen the sideband amplitude is higher than that of the centreband at some defocus values and lower at others. An estimate of the random error in the profiles can be obtained by comparing results obtained at the same defocus of −20 nm at the beginning and the end of the series. Systematic errors, which may also be present, are more difficult to address.

Lattice fringe *contrast* profiles for the sideband and centreband, which were calculated by dividing the amplitudes (Fig. 7) by the mean intensities (Fig. 5), are shown in Fig. 8. Fig. 8 shows that the contrast in the sideband images is greater than that in the centreband images, but that this contrast ratio depends on specimen thickness. At low specimen thickness (from 5 to 15 nm from the specimen edge), the contrast of the sideband images is on average between 1.2 (0 2 0) and 1.4 (2 0 0) times that of the centreband images. Above this thickness, the contrast is on average approximately 1.1 times that of the centreband images for both the 200 and the 020 lattice fringes.

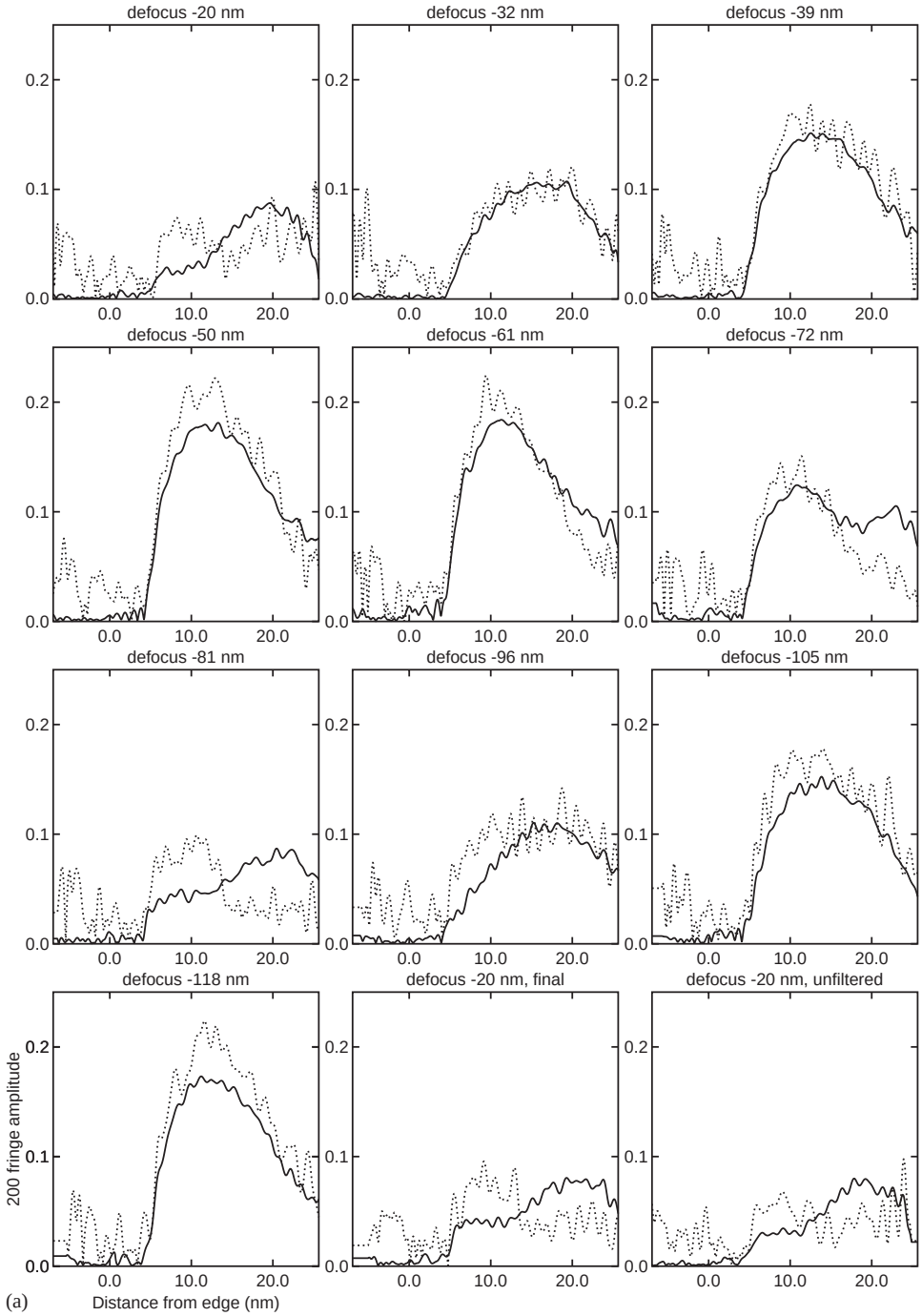

Fig. 6. Lattice fringe amplitudes measured as a function of distance from the specimen edge for the centreband images (solid line) and sideband images (dotted line), for all ten defoci in the focal series and for the initial defocus repeated at the end of the series and an unfiltered image taken at the start of the series. (a) 200 lattice fringe amplitudes and (b) 020 lattice fringe amplitudes.

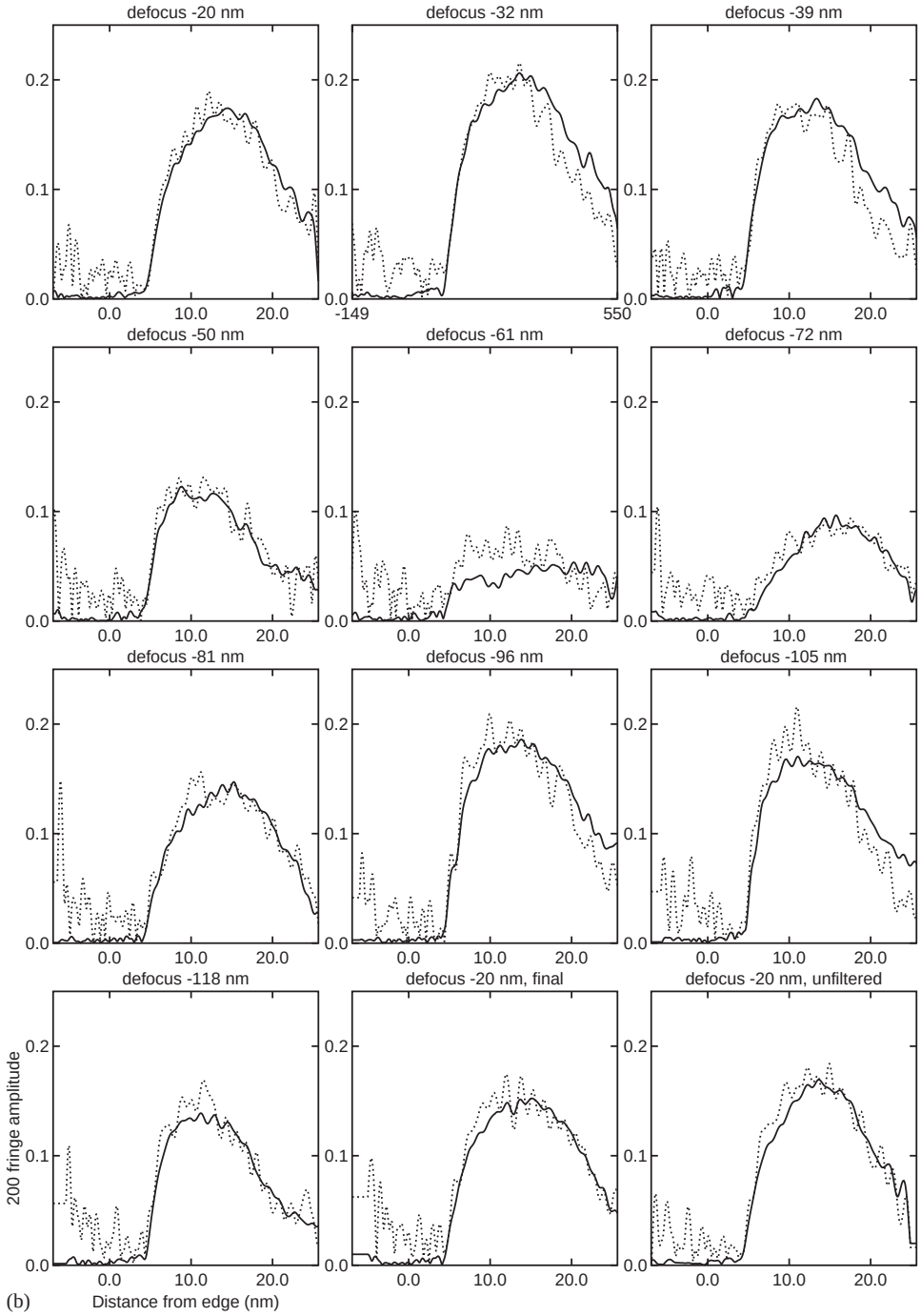

Fig. 6 (*continued*).

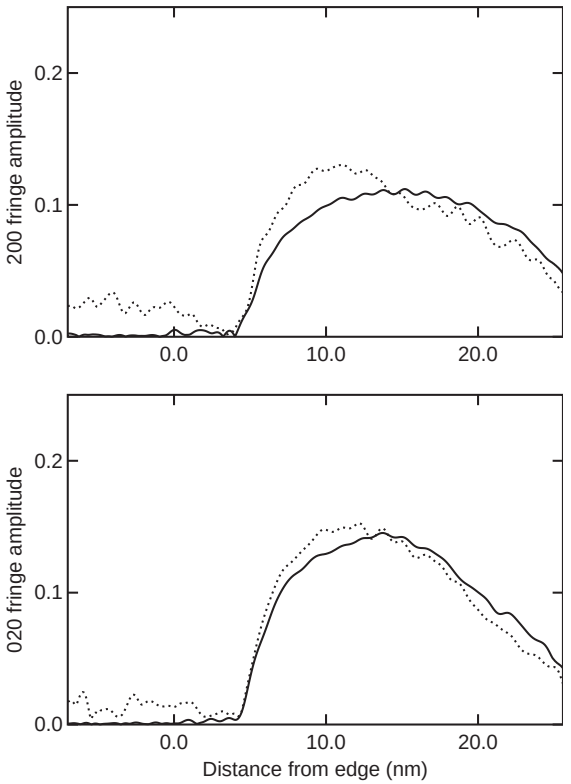

Fig. 7. Average amplitudes of the 200 lattice fringes (top) and 020 lattice fringes (bottom), averaged over all of the defoci shown in Figs. 6a and b, respectively. The averages were performed in the complex plane using the method used to calculate line C in Fig. 3. The centreband and sideband lattice fringe amplitudes are shown as solid and dotted lines, respectively.

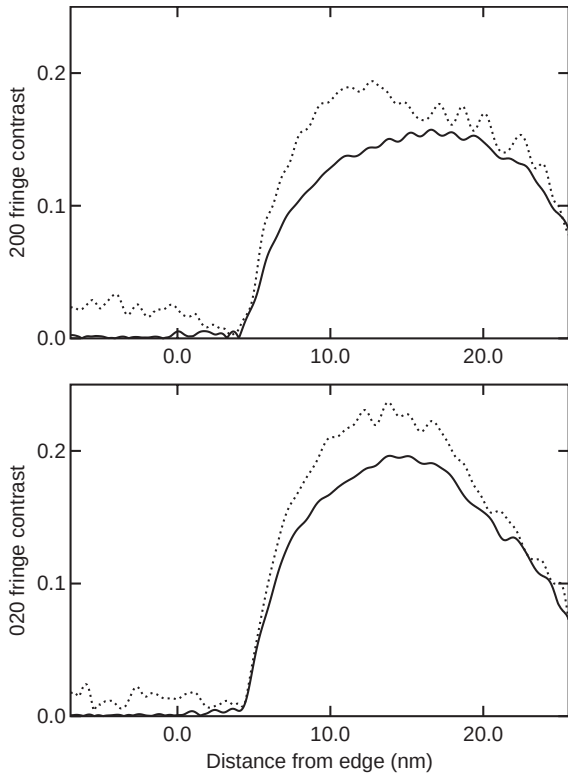

Fig. 8. Average *contrast* of the 200 lattice fringes (top) and 020 lattice fringes (bottom). These profiles were calculated by dividing the average lattice fringe amplitudes shown in Fig. 7 by the mean intensities in Fig. 5. The centreband and sideband contrast are shown as solid and dotted lines, respectively.

6. Discussion

One of the primary advantages of using electron holography to measure phonon scattering is that images that include and exclude phonon-scattered electrons are derived from the same original electron hologram. As a result, any effects that alter the lattice fringe amplitude, such as specimen vibration, objective lens defocus, beam divergence and voltage instabilities, have the same effect on both images. From Fig. 5, it is clear that there is a significant difference in the mean intensities of the sideband and centreband images as a function of specimen thickness. Only electrons with energy losses of up to 5 eV can contribute to the centreband images, which are energy-filtered using a 10 eV energy-selecting slit. As there is very little intensity in the energy-loss spectrum between 0 and 5 eV, it is therefore reasonable to assume that the difference between the sideband and centreband intensities is caused by phonon scattering alone, which contributes only to the centreband.

The possibility of stray scattering, either from the microscope column or from high-angle, low-loss scattering from the specimen (which could contribute to the image due to spherical aberration of the objective lens), must be considered. These effects, which were minimised by using an objective aperture to limit high-angle scattering, were discounted by comparing images taken close to the specimen edge with images taken after the specimen had been moved away from the electron

beam. The possibility of stray scattering in the energy-filter was also discounted by comparing the mean intensities of two images taken with different spectrometer entrance aperture sizes. The absolute vacuum level in the sideband images was determined by using an additional hologram acquired from vacuum alone. Although the holographic interference fringe visibility can differ between successive holograms due to vibrations and instabilities of the microscope and the biprism wire, our measurements suggest that there is no consistent background in the sideband images, and that stray scattering is absent from our data.

We now compare our experimental measurements of mean intensity (Fig. 5), lattice fringe amplitude (Fig. 7) and lattice fringe contrast (Fig. 8) with the schematic diagrams shown in Fig. 4. The lattice fringe amplitudes in unfiltered and energy-filtered images acquired at the same defocus are approximately the same as a function of specimen thickness (e.g., the last two profiles in Figs. 6a and b). As the mean intensity decreases faster with specimen thickness in the energy-filtered than the unfiltered image (Fig. 5), the *contrast* of the energy-filtered image is higher than that of the unfiltered image by an amount that increases with distance from the specimen edge. At a distance of 5 nm from the specimen edge, the contrast in the energy-filtered image is 1.1 times that in the unfiltered image, while at a distance of 15 nm the energy-filtered image has 1.2 times more contrast. The effect of inelastic scattering on an energy-filtered (centreband) image is therefore consistent with the presence of an inelastic background that is proportional to specimen thickness, as shown in Fig. 4b.

At low specimen thickness, the amplitude and the contrast of the 200 and 020 lattice fringes are consistently higher in the sideband images than in the energy-filtered centreband images, up to a distance of approximately 15 nm from the specimen edge (Figs. 7 and 8). As we are certain that stray scattering does not contribute a background to the image (Fig. 4a), these results are consistent with the schematic diagrams shown in Fig. 4d. This situation corresponds to phonon-scattered electrons forming a lattice image that is of opposite sense to the elastic lattice image, and which therefore reduces its amplitude. At a distance of 15 nm from the specimen edge, phonon scattering accounts for up to 15% of the mean intensity in an energy-filtered image, and reduces the lattice fringe amplitude by between 9% and 16%. The lattice image generated by phonon-scattered electrons must therefore have between 60% and 100% of the contrast of the elastic lattice image to provide this reduction in amplitude.

At higher specimen thickness, the sideband amplitude on average decreases below the centreband amplitude, suggesting that the phonon lattice image now has the same sense as the elastic image. The defocus-dependence of this behaviour, which is complicated, can be seen more clearly in Fig. 9. The two columns in this figure correspond to the amplitudes of the 200 and 020 lattice fringes, while each row corresponds to a different specimen thickness. The individual plots show the lattice fringe amplitude plotted as a function of defocus, from a defocus of -20 nm on the left towards increasing underfocus on the right. The two data points on the right of each plot correspond to a return to the initial (-20 nm) defocus value and to an unfiltered image, also acquired at a defocus of -20 nm. In the thinnest part of the crystal, at a distance of 8 nm from the specimen edge (Figs. 9a and b), the sideband amplitude is greater than the centreband amplitude by an amount that is independent of defocus, confirming that phonon-scattered electrons contribute a lattice image that is out of phase with the elastic image at all defoci.

The dependence of the amplitude of the phonon lattice image on defocus in a thin sample is very interesting. In contrast, high-angle annular dark-field (HAADF) images, which are formed largely as a result of phonon scattering, exhibit contrast that decreases rapidly on either side of an optimal defocus value. A direct comparison between these two images is, however, unwarranted because HAADF images are formed as a result of coherent interference between elastically scattered electrons (that have been channelled or dynamically diffracted in the specimen), which is ''transferred'' to the high angle detector by multi-phonon (thermal diffuse) scattering. In our present experiment, for the phonon lattice image to remain out of phase at all defoci, it must undergo the same, or similar,

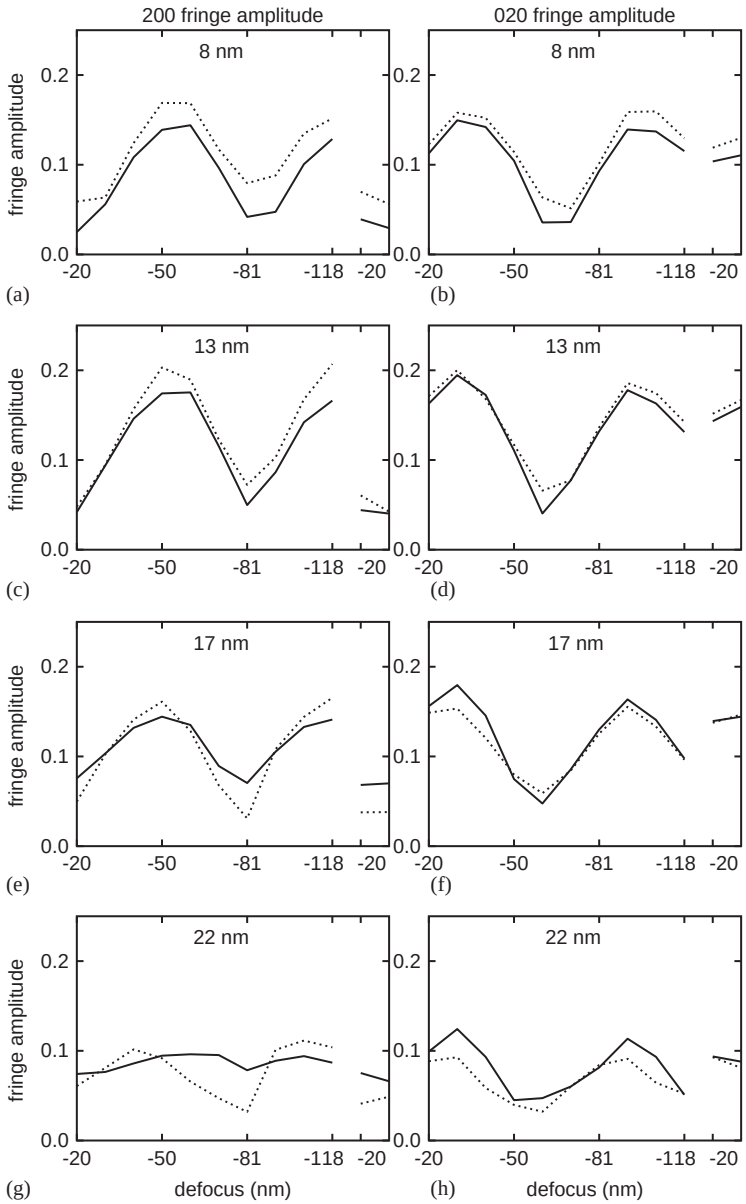

Fig. 9. Defocus-dependence of the lattice fringe amplitude for centreband images (solid line) and sideband images (dotted line). The lattice fringe amplitudes plotted in the four rows are averaged over a distance in each image of 4.7 nm at distances from the specimen edge of (a), (b) 8 nm, (c), (d) 13 nm, (e), (f) 17 nm and (g), (h) 22 nm. The data points on the left of each plot are for the ten images in the focal series from −20 nm to −118 nm in defocus, as in Fig. 6. The two data points on the right are for a return to the initial defocus and for an unfiltered image, also at the initial defocus of −20 nm.

contrast reversals as the elastic lattice image. In the present images, however, only the 200 and 220 beams are allowed to contribute to the phonon lattice image. In addition, the 000 beam is not expected to contribute significantly to the image formed following phonon scattering. Thus, the 200 fringes in the phonon lattice image result primarily from interference between the 200 and 220 beams.

At higher specimen thickness, the behaviour with defocus is more complicated. At a distance of 17 nm from the specimen edge (Figs. 9e and f), the sideband 200 amplitude is greater than the centreband amplitude when the amplitude is high, but the opposite is true when the amplitude is low. However, this behaviour reverses for the 020 fringes. In the thickest part of the crystal, at a distance of 22 nm from the specimen edge (Figs. 9g and h), the sideband and centreband amplitudes have different defocus behaviours. At this sample thickness, phonon-scattered electrons account for 35% of the amplitude of the elastic image. These observations can be compared with the predictions of Rez [12], who calculated phonon lattice images for a [2 0 0] systematic row in a Au specimen of thickness 40 nm. Although the intensity of the phonon lattice image was calculated to be lower than that observed here, both full and half-spacing phonon lattice fringes were predicted.

From our measurement of the phonon contribution to the lattice images (Fig. 5), we can calculate the maximum possible amplitude of the phonon lattice fringes, which can contribute either in phase or out of phase to the elastic image. These two limits are shown in the form of dotted lines in Fig. 10. At each defocus, we can also calculate the amplitude of the phonon lattice fringes by subtracting the sideband (elastic only) amplitude (the dotted lines in Fig. 6) from the centreband (elastic and phonon) lattice fringe amplitude (the solid lines in Fig. 6). These phonon lattice fringe amplitudes are plotted in the form of solid lines in Fig. 10 for the 200 and 020 lattice fringes and for each defocus. If the difference between the centreband and sideband amplitudes is caused by phonon scattering, as we have assumed, then all of the solid lines in Fig. 10 should lie within the limits set by the two dotted lines. Over most of the observed specimen thickness range, this condition is satisfied. However, at low crystal thickness some of the measured amplitudes lie below the lower dotted line, and in the amorphous region most of the amplitudes are too low. In the amorphous region, the low amplitudes result from the greater noise in the sideband lattice fringe amplitudes than in the centreband amplitudes (Fig. 6). Likewise, it is probable that there is enough noise both in the

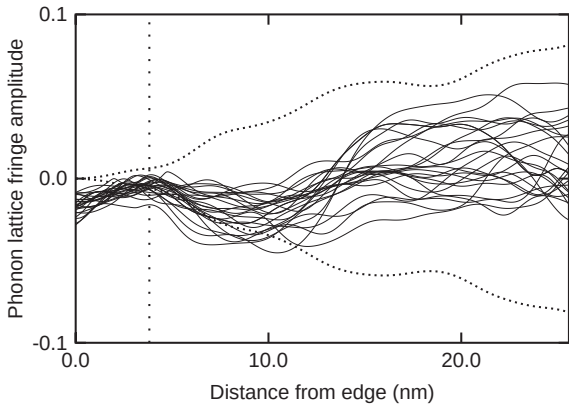

Fig. 10. Amplitude of the phonon lattice fringes. The solid lines show, for the 200 and 020 lattice fringes and for each defocus, the amplitude of the phonon lattice fringes calculated by subtracting the sideband (elastic only) lattice fringe amplitude (as in Fig. 6, dotted lines) from the centreband (elastic and phonon) lattice fringe amplitude (as in Fig. 6, solid lines). The dotted lines show the limits to the possible amplitude of the phonon lattice fringes based on the phonon contribution shown in Fig. 5. Negative lattice fringe amplitudes indicate that the phonon lattice fringes are out of phase with the elastic lattice fringes. The vertical dotted line shows the boundary between the amorphous region (left) and the crystalline region (right).

phonon amplitudes (the solid lines in Fig. 10) and in the maximum phonon amplitudes (the dotted lines in Fig. 10) to account for the lines that lie outside the limits at low crystal thickness. Thus, we are confident that the measured phonon lattice fringe amplitudes (Fig. 6) are consistent with the measured phonon scattering contribution (Fig. 5).

Our observations show that the contributions to a lattice image from both phonon scattering and higher-loss inelastic scattering increase in proportion to specimen thickness. The phonon contribution is very low in the amorphous layer at the edge of the sample, while the inelastic contribution is much more significant in this region. Thus, in an energy-filtered lattice image, the primary cause of contrast reduction in the thinnest regions of the sample is associated with diffuse (elastic) scattering from the amorphous layer, with the contrast then reducing (and the Stobbs factor increasing) as the specimen thickness increases. Fig. 11 summarises the measured effect of phonon scattering as a function of distance from the specimen edge. The lines show the ratio of the lattice fringe contrast in

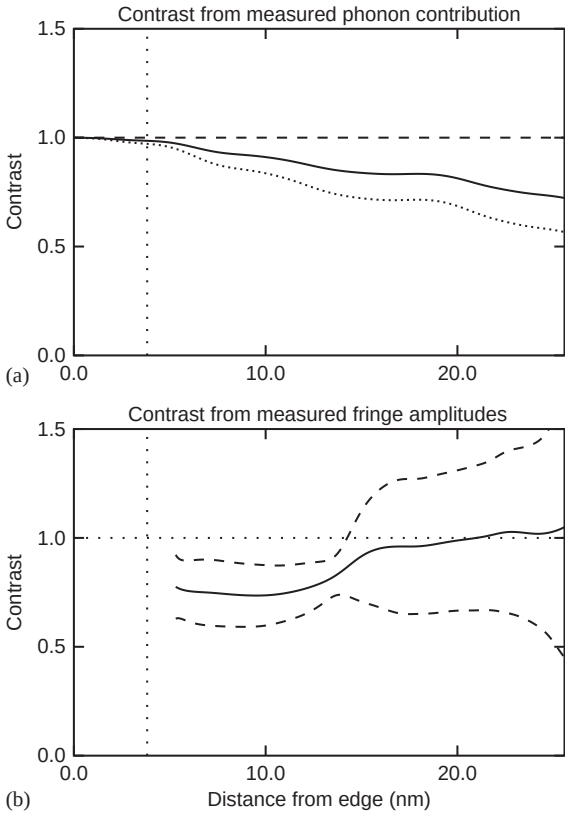

Fig. 11. The amount by which phonon scattering reduces the lattice fringe contrast. The lines show the ratio of the lattice fringe contrast in an image containing phonon scattering to the lattice fringe contrast in a purely elastic image. (a) The effect of the measured phonon contribution (Fig. 5) on the lattice fringe contrast. The solid line corresponds to phonon scattering adding a constant background to the lattice image, as in Fig. 4b. The dashed line corresponds to phonon scattering adding a lattice image identical to the elastic lattice image, as in Fig. 4c. The dotted line corresponds to phonon scattering adding a lattice image that is out of phase with the elastic lattice image, as in Fig. 4d. (b) shows the effect of phonon scattering on the measured lattice fringe contrast (Fig. 6). The solid line shows the ratio of the lattice fringe contrast in images containing phonon scattering (centreband) to the lattice fringe contrast in images with no phonon scattering (sideband), averaged over all defoci and over the 200 and 020 lattice fringes. The dashed lines show one standard deviation on either side of the mean. The vertical dotted line shows the boundary between the amorphous region (left) and the crystalline region (right), while the horizontal dotted line corresponds to no change in contrast.

an image containing phonon scattering (centreband image) to the lattice fringe contrast in a purely elastic image (sideband image), and thus show the amount by which phonon scattering reduces the lattice fringe contrast. Fig. 11a shows the limits on the effect that phonon scattering (Fig. 5) can have on lattice fringe contrast, based on the measurements of mean intensity alone. The three lines represent the limiting cases when phonon scattering adds a constant background to the lattice image, as in Fig. 4b (solid line), when its adds a lattice image identical to the elastic lattice image, as in Fig. 4c (dashed line) and when it adds a lattice image out of phase with the elastic lattice image, as in Fig. 4d (dotted line). As expected, there is very little contrast reduction due to phonon scattering in the amorphous layer, and the contrast reduction increases with specimen thickness. An inherent assumption in Fig. 11a is that the contrast of the lattice fringes in the phonon lattice image is similar to that in the elastic lattice image. This assumption is untrue at low specimen thickness, when the elastic lattice fringe amplitude is small. For example, at defoci of -20 and -81 nm in Fig. 6a the lattice image containing phonon scattering has only half of the contrast of the elastic image at low specimen thickness, which is outside the range predicted by Fig. 11a. Thus, there are situations when the elastic lattice fringe contrast is at a minimum and phonon contrast begins to dominate the image.

Fig. 11b shows an alternative measure of the reduction in contrast caused by phonon scattering. The solid line in Fig. 11b is the ratio of the lattice fringe *contrast* in images containing phonon scattering (centreband) to the lattice fringe *contrast* in images with no phonon scattering (sideband), averaged over all defoci and over the 200 and 020 lattice fringes. Because there is a large spread in this measurement with defocus, the two dashed lines are included to show one standard deviation on either side of this average. Fig. 11b shows that at low specimen thickness phonon scattering reduces the lattice fringe contrast to $\sim$75% of that in an elastic lattice image, while at higher specimen thickness there is little reduction in lattice fringe contrast by phonon scattering on average, but a large spread over individual defocus values. Interestingly, in Fig. 11b phonon scattering causes the greatest reduction in lattice fringe contrast at low specimen thickness, in

contradiction to Fig. 11a. The examination of both Fig. 11a and Fig. 11b, alongside the previous figures, suggests that at certain sample thicknesses and defocus values the phonon lattice image can have greater contrast that that of the elastic image.

7. Conclusions

Off-axis electron holography combined with energy-filtered imaging has been used to measure the effect of phonon scattering on the contrast of high-resolution lattice images of ZrB_{12}. For this material, the phonon contribution to the background level in an unfiltered lattice image is only slightly smaller than the contribution from higher-loss inelastic scattering. Although the amorphous layer at the specimen edge makes a comparatively large contribution to the inelastic scattering in the image, very little phonon scattering occurs within this layer. Phonon scattering *reduces* the *amplitude* of the lattice fringes in a thin sample, which suggests that it provides lattice fringes of opposite sense to the elastic lattice image. In a thicker sample, the phonon contribution becomes dependent on both specimen thickness and defocus. It therefore affects the pattern of the fringes in a lattice image, complicating attempts to match experimental results with image simulations.

The proportion of phonon-scattered electrons at a typical specimen thickness used for HREM imaging accounts for 15% of the mean intensity in the image (Fig. 5), which is not enough on its own to account for a Stobbs factor of 2–3. However, at this specimen thickness phonon scattering adds not just a uniform background, but a lattice image of opposite sense to the elastic lattice image. The lattice fringe contrast in an energy-filtered image can then be reduced to 70% of its expected value by phonon scattering, which would correspond to a Stobbs factor of 1.4. The amount of phonon scattering is found to be proportional to specimen thickness, and cannot account for Stobbs factors of two to three observed in the thinnest parts of specimens [3]. However, the *combined* effect of phonon scattering and scattering from amorphous surface layers (present even in the thinnest regions of the sample) may be sufficient to account for the Stobbs factor in many materials.

Acknowledgements

We acknowledge useful discussions with Christian Dwyer, Archie Howie, Koji Kimoto, Angus Kirkland, Michael Lehmann, Paul Midgley, Alex Moodie, Dirk van Dyck, and in particular Kazuo Ishizuka, Rüdiger Meyer and Peter Rez. We are very grateful to Akira Tonomura and Ken Harada for their hospitality at the Hitachi Advanced Research Laboratory, where much of the analysis for this paper was carried out, and to Colin Kennard and Alex Moodie for providing the ZrB_{12} sample. RDB thanks the Royal Society for financial support.

References

[1] C.B. Boothroyd, J. Microsc. 190 (1998) 99.
[2] M.J. Hytch, W.M. Stobbs, Ultramicroscopy 53 (1994) 191.
[3] C.B. Boothroyd, R.E. Dunin-Borkowski, W.M. Stobbs, C.J. Humphreys, Beam-solid interactions for materials synthesis and characterization, in: D.C. Jacobson, D.E. Luzzi, T.F. Heinz, M. Iwaki (Eds.), Materials Research Society Symposium Proceedings, Vol. 354, Materials Research Society, Pittsburgh, 1995, pp. 495–500.
[4] C.B. Boothroyd, Ultramicroscopy 83 (2000) 159.
[5] C.B. Boothroyd, M. Yeadon, Ultramicroscopy 96 (2003) 361–365.
[6] W.M. Stobbs, W.O. Saxton, J. Microsc. 151 (1987) 171.
[7] C.B. Boothroyd, W.M. Stobbs, Ultramicroscopy 26 (1988) 361.
[8] C.B. Boothroyd, W.M. Stobbs, Ultramicroscopy 31 (1989) 259.
[9] K. Kimoto, Y. Matsui, J. Electron Microsc. 50 (2001) 377.
[10] S.J. Lloyd, R.E. Dunin-Borkowski, C.B. Boothroyd, Inst. Phys. Conf. Ser. 153 (1997) 113.
[11] J.M. Cowley, Acta Crystallogr. A 44 (1988) 847.
[12] P. Rez, Ultramicroscopy 52 (1993) 260.
[13] Z.L. Wang, Philos. Mag. B 79 (1999) 37.
[14] F. Loane, P. Xu, J. Silcox, Acta Crystallogr. A 47 (1991) 267.
[15] C. Dwyer, J. Etheridge, Ultramicroscopy (2003), in press.
[16] D.A. Muller, B. Edwards, E.J. Kirkland, J. Silcox, Ultramicroscopy 86 (2001) 371.
[17] A. Tonomura, Adv. Phys. 41 (1992) 59.
[18] D. van Dyck, H. Lichte, J.C.H. Spence, Ultramicroscopy 81 (2000) 187.
[19] F. Zhou, Ultramicroscopy 92 (2002) 293.

[20] J.C.H. Spence, J.M. Zuo, Ultramicroscopy 69 (1997) 185.
[21] M. Lehmann, D. Geiger, I. Büscher, H.W. Zandbergen, D. van Dyck, H. Lichte, in: Proceedings of the 15th International Congress on Electron Microscopy, Vol. 3, Durban, 2002, pp. 279–280.
[22] C.H.L. Kennard, L. Davis, J. Solid State Chem. 47 (1983) 103.
[23] A. Leithe-Jasper, A. Sato, T. Tanaka, Z. Kristallogr. NCS 217 (2002) 319.
[24] R.R. Meyer, A.I. Kirkland, W.O. Saxton, Ultramicroscopy 92 (2002) 89.
[25] W.J. de Ruijter, P.E. Mooney, E. Völkl, Mater. Soc. Am. Bull. 24 (1994) 451.
[26] R.R. Meyer, A.I. Kirkland, R.E. Dunin-Borkowski, J.L. Hutchison, Ultramicroscopy 85 (2000) 9.
[27] S.J. Pennycook, D.E. Jesson, Ultramicroscopy 37 (1991) 14.